Limerick Wave: using flywheel technology to convert the power of the waves to electricity

Burns, Shane
S.Burns3@nuigalway.ie

Chapwanya, Michael
Michael.Chapwanya@up.ac.za

Cummins, Cathal*
Cathal.Cummins@ul.ie

Dellar, Paul
dellar@maths.ox.ac.uk

Giddings, Joe
pmxjag@nottingham.ac.uk

Giounanlis, Panagiotos
panagiotis.giounanlis@ucdconnect.ie

Hicks, Peter
P.Hicks@abdn.ac.uk

McCarthy, Jack
12148288@studentmail.ul.ie

McGinty, Sean
s.mcginty@strath.ac.uk

Moroney, Kevin
Kevin.Moroney@ul.ie

Nicholson, Michael
s0832996@sns.ed.ac.uk

O'Brien, Stephen
stephen.obrien@ul.ie

Pawłowska, Bogna
bognabognabogna@gmail.com

Richter, Ruan
10130306@studentmail.ul.ie

Foged Schmidt, Marie
s082746@student.dtu.dk

Thomas, Gareth
ThomasGP@ucc.ie

Vynnycky, Michael
michael.vynnycky@ul.ie

Yavuz, Burak
brkyvz@gmail.com

August 22, 2013

Executive summary

Limerick Wave Ltd. has developed an innovative wave energy converter (WEC) technology. They use a recently-patented flywheel technology to use the power from the movement of the waves (via the movement of a cylindrical floatation device) to generate electricity. The use of flywheel technology in this area is novel in that its rotation is unidirectional despite the bi-directional natural oscillation of the floatation device.

In this report a mathematical description (model) of the WEC device's operations is presented. Limerick Wave's current experimental prototype is a 1:20 model; this model serves as a way to check the performance of a scaled-up rig. The model allows Limerick Wave to fine-tune their device's design in order to maximise, say, the energy extracted from the ocean waves.

By applying standard physical laws (conservation of angular momentum etc.) to the device's operation, we show that such a device will demonstrate periodic behaviour regardless of its initial orientation. A crucial finding of the report concerns the power take-off mechanism. We identify two qualitatively different operational states: the first (second) state corresponds to extracting a small (large) amount of energy per cycle. Each operational state has its own benefits and shortcomings – these are examined in detail in the report.

We perform a preliminary run of device-tuning; we take data from the observation buoys in Galway Bay to compute an optimum arm length for the device for harnessing power from the ocean. The data contains a strong seasonal variance and this is incorporated into the optimisation.

*Please send any correspondences to this author.

1 Introduction

The world's energy consumption is estimated to rise considerably over the next decades and, in light of the constant reminders of the environmental impact of some of the traditional methods of energy production, governments have seen the urgent need for pollution-free power generation [2]. One of the renewable energies being investigated is wave power and the development of efficient wave energy converters (WECs).

The idea of wave energy extraction is not new, in fact it is at least two centuries old. The possibility that wave energy could be converted into usable energy has inspired numerous inventors and resulted in countless inventions. The earliest such invention to be patented was made in France in 1799 and by 1980 more than one thousand such patents had been registered [3]. With increased funding being put into research and development projects worldwide, and particularly in the EU, this number is ever increasing.

The global power potential represented by waves that hit all coasts worldwide has been estimated to be in the order of one terawatt ($\sim 10^{12}$ W) [4]. If wave energy is harvested on the open ocean, energy that is otherwise lost in friction and wave breaking may be utilised and the previous estimate increases by one order of magnitude ($\sim 10^{13}$ W). This figure is comparable with the present world power consumption. An important feature of sea waves is that they have the highest energy density among the renewable energies [2]. Wave energy is derived from winds which blow across the oceans. As wind energy is converted to wave energy the average power flow intensity increases from $\sim 0.5\,\mathrm{kW/m^2}$ to $\sim 3\,\mathrm{kW/m^2}$ [4]. Certain geographical areas also have higher wave power levels than others. Averaged over years, offshore wave power levels of $30-100\,\mathrm{kW/m}$ are found at latitudes $40^\circ - 50^\circ$ and less power further north and south [4]. In terms of wave energy generation potential, this is very encouraging from an Irish and European prospective. In particular, power levels[1] of up to $75\,\mathrm{kW/m}$ have been assigned to areas off Ireland and Scotland.

Despite all the recent investment in wave power, the worldwide installed capacity of wave power remains stubbornly low. Thus it is important to ask why. Clément *et al.* [2] identifies three key difficulties facing wave power development:

1. Irregularity in wave amplitude, phase, and direction: it is difficult to obtain maximum efficiency of a device over the entire range of excitation frequencies.

2. The structural loading in the event of extreme weather conditions, such as hurricanes, may be as high as 100 times the average loading.

3. The coupling of the irregular, slow motion (frequency $\sim 0.1\,\mathrm{Hz}$) of a wave to electrical generators requiring typically ~ 500 times greater frequency.

The power take-off mechanism (PTO) should allow the production of usable energy [4, 3]. However, the barrier to this goal is that the wave power varies on several scales: wave periods, hours, days, weeks, seasons, and years.

Currently there is a wide variety of wave energy technologies and recent reviews have identified about one hundred projects at various stages of development. Falcão [3] contains descriptions of some of these technologies. The WEC system developed by Limerick Wave has a number of distinguishing and innovative features. Unlike many other WEC devices, the device of Limerick Wave incorporates a mechanical power take off, rather than a hydraulic power take off. The oscillatory motion of a cylindrical floatation device, connected to a gear box by a rigid arm, is used to drive a gearbox. Inside the gear box the low frequency oscillations are ramped up to high frequencies by specifying the gear ratio. The bi-directional natural oscillations of the floatation device are also rectified by a mechanical diode within the gearing. The rectified output then drives the flywheel. This patented flywheel system can be used as a capacitor to store and smooth the energy supplied to the generator. For example when the energy input to the system is large the flywheel can be used to store energy and then when energy input is low, the flywheel can supply energy to the generator. The system also features a 360° driving arc making it robust to storm conditions, which present a problem to some other WECs. An illustration of the WEC device is shown in Figure 1. The main cylindrical unit of the device, which consists of a generator connected to the gearing system to generate energy from mechanical advantage of the flywheel, is mounted on a frame which is moored to the seabed.

[1] This quantity is the amount of power per unit of wave-crest length [5]; hence, the quantity $75\,\mathrm{kW/m}$ means there are 75 kilowatts of power potential per meter of wave crest.

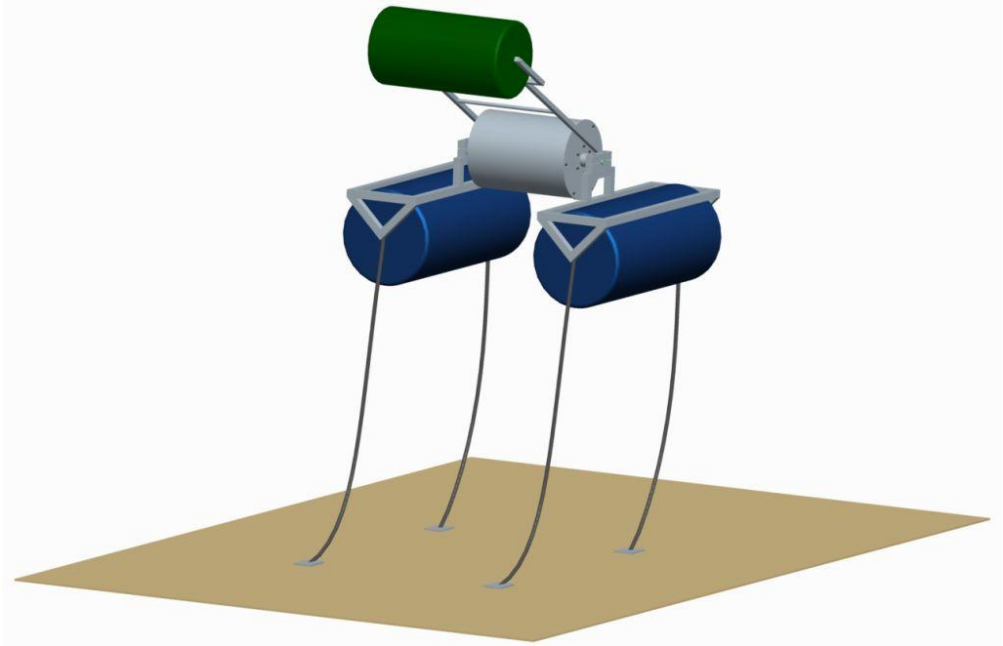

Figure 1: Illustration of WEC device moored to seabed.

All the necessary controls are housed within the sealed cylindrical unit. The WEC device can be placed beneath or sitting on the water while the cylindrical floats rests in the water. Limerick Wave claim their device offers five key advantages over existing designs:

1. Energy is fed to the flywheel within the sealed cylindrical unit by the forward and reverse rotating cylinder due to the reciprocating motion of the water surface. The rotation of the flywheel is unidirectional despite the rotation of the cylinder being bi-directional. This design can have more than one generator within the sealed unit, enabling it to deal with changing energy input levels.

2. The main body of the unit can be below sea level, protecting it from the harshness of the environment.

3. The wave energy conversion device houses the primary converter; the PTO system and the energy is converted to electrical energy within the sealed unit. This sealed unit provides a protected environment for the control and optimisation of the energy from the flywheel. The main or expensive components are housed within the sealed unit. The use of a flywheel is an efficient way of storing energy and smoothing out the input.

4. Supercapacitor lifetime issues seriously limit the application of wave energy power smoothing, and to fulfil power smoothing requirements it is necessary to use kinetic energy storage of high speed inertia. The flywheel used in the PTO system addresses this concern.

5. This is a power take-off unit, which is missing within the industry. In proving this concept a major deficiency in the industry will be addressed.

In general the development of such a concept to the commercial stage has been found to be difficult, slow, and expensive [3]. Thus the use of mathematical and numerical modelling can be very useful to determine, first of all the viability of a system, and then the optimal combination of system parameters to achieve the best results. Such results are extremely valuable before investing in designing and building large scale models. In the Limerick Wave case, three main challenges have been presented to the Study Group:

1. Develop a hydrodynamic model for an incoming regular wave.

2. Provide a model of the power take-off mechanism.

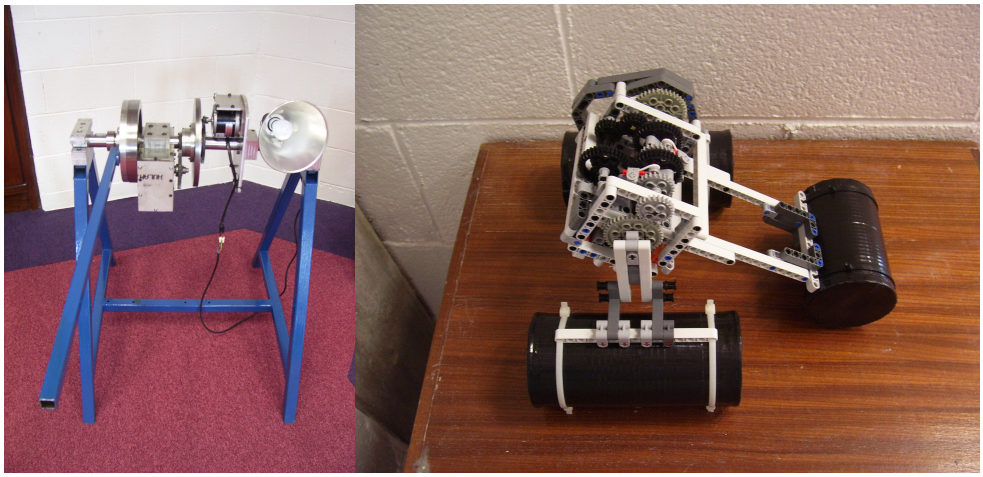

Figure 2: Left: scaled version of Limerick Wave's WEC device. Right: miniature working model of Limerick Wave's floating WEC device with mechanical diode

3. Examine how the hydrodynamic model and mechanical model can be combined; in particular whether they can be combined in a linear way, or whether a non-linear approach is required.

While this report focuses mainly on the second challenge, it deals with aspects of all three.

2 Model formulation

We model Limerick Waves's WEC device as a generator, which is mounted on a frame moored to the seabed, connected through a gearing system to a flywheel. The flywheel is driven by a rigid arm with a floatation device connected to its end that, in turn, follows the ocean's waves. The arm is free to move in a full 360° rotation about its pivot point in the frame. Due to the presence a mechanical rectifier in the gearing, the rotation of the flywheel is unidirectional despite the rotation of the arm being bi-directional.

Let the quiescent height of the sea be located a distance Y above the centre of the flywheel/gearbox as shown in Figure 3. Attached to the flywheel is an arm of length L which is, in turn, connected to a floating device – in this case a cubic box of side length H. The angle $\theta(t)$ is the angle that the arm makes with the horizontal, which will be a function of time. The wave is assumed to be a sinusoidal displacement, $h(t) = \ell \sin \Omega t$, of the sea surface from its quiescent height, where ℓ is the wave amplitude and Ω is the wave frequency. We assume here that the motion of the float and the flywheel do not affect the wave train. The movement of the arm causes rotation of the flywheel through a gearbox in the device – the angular velocity of the flywheel is $\omega(t)$.

The acceleration of the float (density ρ_f) is determined by a balance of buoyancy (water density ρ_w) and weight as shown in Figure 3. The buoyancy takes a maximum value when the float becomes totally submerged and tends to zero as the float exits the water. For simplicity the float is assumed to be rectangular, rather than the cylindrical shape envisaged by Limerick Wave. At the current level of analysis this choice makes no difference to the dynamics. However, for future deployment, careful consideration should be given to the float shape: particularly to reduce impact pressures if the float leaves and re-enters the water [6]. As the float moves according to this force balance it generates a torque on the arm of the device which, in turn, spins the flywheel as shown in Figure 4.

2.1 Conservation of angular momentum

By the conservation of angular momentum, the sum of the torques about a point should be proportional to the angular acceleration

$$Ia = \sum \tau. \tag{1}$$

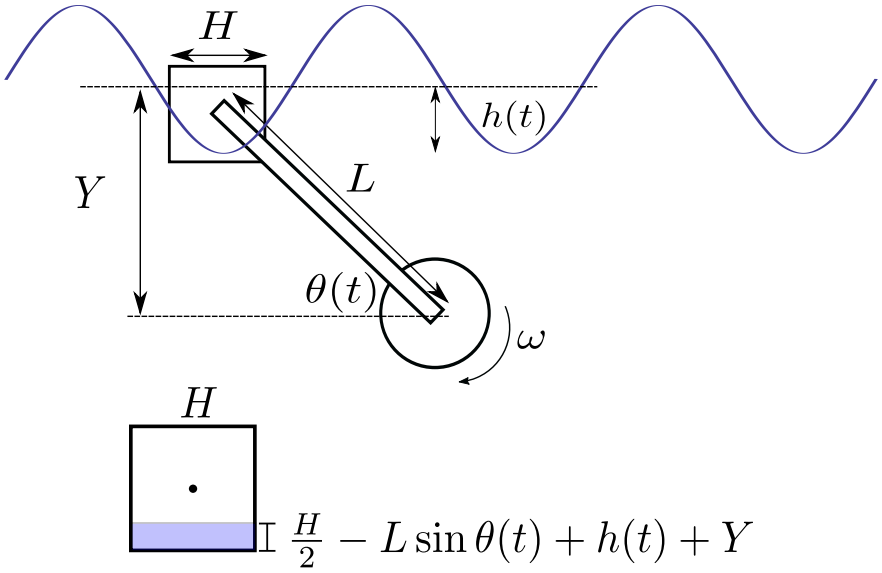

Figure 3: Top: model definitions and WEC schematic. Bottom: buoyancy force on float due to partially submerged volume.

Consider the float's angular momentum about its mount point, which comprises the torque due to the buoyancy of the float and the torque due to the gearing

$$I_{\text{arm}}\ddot{\theta} = \tau_{\text{float}} - \text{sign}\left(\dot{\theta}\right)\tau_{\text{gear}}, \tag{2}$$

where a dot above a variable indicates differentiation with respect to time. The flywheel's angular momentum comprises the torque due to the gearing and the torque due to the generator

$$I_{\text{fly}}\dot{\omega} = \tau_{\text{gear}} + \tau_{\text{gen}}, \tag{3}$$

where I_{arm} is the moment of inertia of the arm and I_{fly} is the moment of inertia of the flywheel (incorporating the gear ratio).

The torque due to the float is given by the equation

$$\tau_{\text{float}} = \left[\min\left(\max\left(\frac{H}{2} + Y - L\sin\theta + h(t),\, 0\right),\, H\right) A\rho_w g - \rho_f g H A\right] L\cos\theta, \tag{4}$$

where A is the area of the bottom surface of the float and g is the acceleration due to gravity. Here the minimum and maximum functions account for the fact that the vertical height of the submerged float varies between 0 (when the float is out of the water) and H (when the float is completely submerged).

The torque extracted by the generator is taken to be proportional to the angular velocity ω of the flywheel

$$\tau_{\text{gen}} = -k\omega, \tag{5}$$

for a constant resistive load. The torque transmitted through the gears is

$$\tau_{\text{gear}} = \frac{1}{\beta}\mathcal{H}\left(|\dot{\theta}| - \omega\right)\left(|\dot{\theta}| - \omega\right), \tag{6}$$

where β is related to the elasticity of the gear teeth and $\mathcal{H}(s)$ is the Heaviside step function[2]. Consider (6) in the small-β limit and consider the two cases separately: when the gears are engaged and when they are not engaged.

[2] The $|\dot{\theta}|$ appearing in (6) is due to the device's mechanical rectifier.

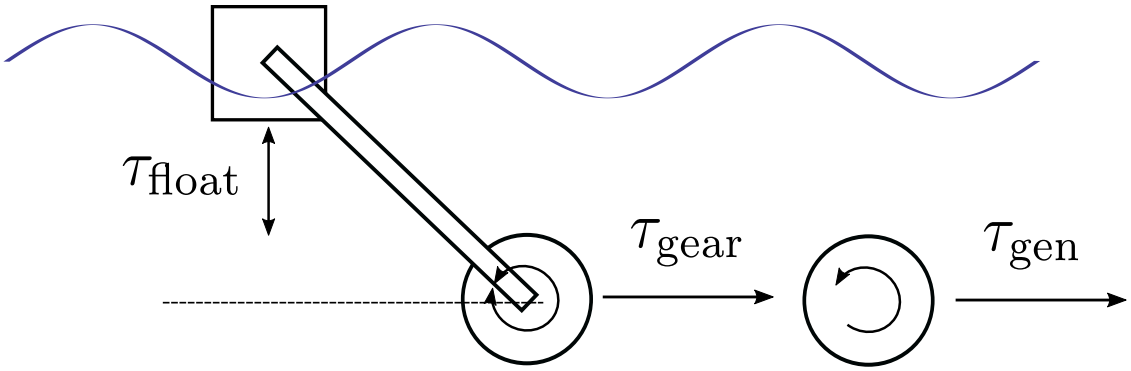

Figure 4: Torque generation by wave transmitted through flywheel to the electrical generator.

When the gears engage, the angular velocity of the flywheel is equal to the rectified angular velocity of the arm: $\omega = m|\dot{\theta}|$ from (6). Once the gears are engaged, then, τ_{gear} may be removed from equations (2) and (3). The equations (2) and (3) may then be added, giving the equation

$$(I_{\text{fly}} + I_{\text{arm}})\,\ddot{\theta} = \tau_{\text{float}} + \tau_{\text{gen}}. \tag{7}$$

If the gears are not engaged, then $|\dot{\theta}| < \omega$, and from (6) no torque gets transmitted through the gears: $\tau_{\text{gear}} = 0$. In this case (2) and (3) decouple into

$$I_{\text{arm}}\ddot{\theta} = \tau_{\text{float}}, \tag{8}$$

for the float, and

$$I_{\text{fly}}\dot{\omega} = \tau_{\text{gen}}, \tag{9}$$

for the flywheel.

2.2 Non-dimensionalisation

Let T be the characteristic timescale for the problem; we scale the time variable to $t = Tt^*$ and we scale the angular velocity to $\omega = \frac{1}{T}\omega^*$. As in Subsection 2.1, we treat separately the cases of engaged gears and disengaged gears.

If we drop the asterisks (which indicate dimensionless variables), then in the engaged case where $\omega = |\dot{\theta}|$, we have

$$\frac{I_{\text{fly}}}{T^2}\left(1 + \frac{I_{\text{arm}}}{I_{\text{fly}}}\right)\ddot{\theta} = A\rho_w gLH\left[\min\left(\max\left(\frac{1}{2} + \frac{Y}{H} - \frac{L}{H}\sin\theta + \frac{\ell\sin(\Omega Tt)}{H},\, 0\right),\, 1\right) - \frac{\rho_f}{\rho_w}\right]\cos\theta - \frac{mk}{T}\omega, \tag{10}$$

while in the disengaged case where $|\dot{\theta}| < \omega$,

$$\frac{I_{\text{arm}}}{T^2}\ddot{\theta} = A\rho_w gLH\left[\min\left(\max\left(\frac{1}{2} + \frac{Y}{H} - \frac{L}{H}\sin\theta + \frac{\ell\sin(\Omega Tt)}{H},\, 0\right),\, 1\right) - \frac{\rho_f}{\rho_w}\right]\cos\theta, \tag{11a}$$

$$\frac{I_{\text{fly}}}{T^2}\dot{\omega} = -\frac{k}{T}\omega. \tag{11b}$$

Taking as the timescale

$$T = \sqrt{\frac{I_{\text{fly}}}{A\rho_w gL^2}}, \tag{12}$$

and defining a non-dimensional wave frequency

$$\Omega_w = \Omega T, \tag{13}$$

we get:

$$\begin{cases} \left(1+\frac{I_{\text{arm}}}{I_{\text{fly}}}\right)\ddot{\theta} = \frac{H}{L}\left[\min\left(\max\left(\frac{1}{2}+\frac{Y}{H}-\frac{L}{H}\sin\theta+\frac{\ell\sin(\Omega_w t)}{H},\,0\right),\,1\right)-\frac{\rho_f}{\rho_w}\right]\cos\theta-\frac{k}{\sqrt{AI_{\text{fly}}\rho_w g L^2}}\omega & \text{if } \omega=|\dot{\theta}|, \\ \frac{I_{\text{arm}}}{I_{\text{fly}}}\ddot{\theta} = \frac{H}{L}\left[\min\left(\max\left(\frac{1}{2}+\frac{Y}{H}-\frac{L}{H}\sin\theta+\frac{\ell\sin(\Omega_w t)}{H},\,0\right),\,1\right)-\frac{\rho_f}{\rho_w}\right]\cos\theta; \quad \dot{\omega}=-\frac{k}{\sqrt{AI_{\text{fly}}\rho_w g L^2}}\omega & \text{if } |\dot{\theta}|<\omega. \end{cases} \tag{14}$$

Defining the ratio of the moments of inertia

$$\delta = \frac{I_{\text{arm}}}{I_{\text{fly}}},$$

a PTO coefficient

$$\alpha = \frac{k}{\sqrt{AI_{\text{fly}}\rho_w g L^2}},$$

non-dimensional length ratios

$$\epsilon = \frac{H}{L},\ \gamma = \frac{Y}{H},\ \eta = \frac{\ell}{H}, \tag{15}$$

and the ratio of float density to liquid density

$$r = \frac{\rho_f}{\rho_w},$$

gives

$$\begin{cases} (1+\delta)\ddot{\theta} = \epsilon\left[\min\left(\max\left(\frac{1}{2}+\gamma-\frac{1}{\epsilon}\sin\theta+\eta\sin(\Omega_w t),\,0\right),\,1\right)-r\right]\cos\theta-\alpha\omega & \text{if } \omega=|\dot{\theta}|, \\ \delta\ddot{\theta} = \epsilon\left[\min\left(\max\left(\frac{1}{2}+\gamma-\frac{1}{\epsilon}\sin\theta+\eta\sin(\Omega_w t),\,0\right),\,1\right)-r\right]\cos\theta; \quad \dot{\omega}=-\alpha\omega & \text{if } |\dot{\theta}|<\omega. \end{cases} \tag{16}$$

In this non-dimensionalisation the quantity $\min\left(\max\left(\frac{1}{2}+\gamma-\frac{1}{\epsilon}\sin\theta+\eta\sin(\Omega_w t),\,0\right),\,1\right)$ has the physical interpretation of being the vertical proportion of the float that is submerged at a given time. This is bounded below by zero (for a float entirely above the water surface), and above by one (for a fully submerged float).

For Limerick Wave's particular WEC device, one might expect the moment of inertia of the float to be much greater than the moment of inertia of the flywheel, which would give rise to a value of $\delta \gg 1$. However, encapsulated within I_{fly} is the gearing ratio and with this included, it is instead expected that δ is a comparatively small parameter within these equations.

In the case where the float remains strictly partially submerged throughout its evolution, the equations of motion can be simplified to give

$$\begin{cases} (1+\delta)\ddot{\theta} = \epsilon\left[\frac{1}{2}+\gamma-\frac{1}{\epsilon}\sin\theta+\eta\sin(\Omega_w t)-r\right]\cos\theta-\alpha\omega & \text{if } \omega=|\dot{\theta}|, \\ \delta\ddot{\theta} = \epsilon\left[\frac{1}{2}+\gamma-\frac{1}{\epsilon}\sin\theta+\eta\sin(\Omega_w t)-r\right]\cos\theta; \quad \dot{\omega}=-\alpha\omega & \text{if } |\dot{\theta}|<\omega. \end{cases} \tag{17}$$

2.3 Numerical scheme

In both the coupled and uncoupled cases, an angular velocity for the float, ϕ, is defined, which allows the second order ordinary differential equation for the angular acceleration to be expressed as a pair of first order ordinary differential equations. In the coupled ($\omega = |\dot{\theta}|$) case this system is

$$\begin{cases} (1+\delta)\dot{\phi} = & \epsilon\left[\min\left(\max\left(\frac{1}{2}+\gamma-\frac{1}{\epsilon}\sin\theta+\eta\sin(\Omega_w t),\,0\right),\,1\right)-r\right]\cos\theta-\alpha\omega, \\ \dot{\theta} = & \phi, \end{cases} \tag{18}$$

while in the uncoupled ($\omega < |\dot{\theta}|$) case

$$\begin{cases} (1+\delta)\,\dot{\phi} = & \epsilon\left[\min\left(\max\left(\frac{1}{2}+\gamma-\frac{1}{\epsilon}\sin\theta+\eta\sin(\Omega_w t)\,,\,0\right),\,1\right)-r\right]\cos\theta, \\ \dot{\theta} = & \phi, \\ \dot{\omega} = & -\alpha\omega. \end{cases} \tag{19}$$

If the WEC was restricted to purely coupled or uncoupled dynamics, then these equations could be readily solved using standard ordinary differential equation solving techniques. However, the switching between coupled and uncoupled dynamics complicates the numerical solution procedure.

To illustrate how the switching mechanism is implemented, the numerical procedure is now described:

1. At the beginning of each time step the motion of the float and flywheel are first calculated using the system (19) for uncoupled motion, which generates a first possible solution.
2. This possible solution is then tested:
   - If $|\dot{\theta}| < \omega$, then this is a valid solution, which is accepted as the updated system position and we return to step 1 to calculate the next time step.
   - However, if $|\dot{\theta}| > \omega$, then the solution generated by step 1 is rejected as being unphysical, as the float has moved faster than the gearing system allows. In this case the gearing must have engaged and the coupled dynamics are appropriate.
3. We now return to the system position at the beginning of the time step and advance the system based on the coupled dynamics (18).

A second order Runge-Kutta scheme with fixed time step is used to perform the integration of both the coupled and uncoupled systems. Results for this numerical system are presented in Section 3.

2.4 Alternative formulation

An alternative formulation of the problem discussed above will be given in detail in this section. In particular we aim to solve the ODE system in its entire form without having to switch between two ODEs depending on the sign of $\omega - |\dot{\theta}|$. We summarise the system of equations as follows

$$(1+\delta)\ddot{\theta} = \epsilon(B-r)\cos\theta - \text{sign}(\dot{\theta})\tau_{\text{gear}}, \tag{20}$$

$$\dot{\omega} = \tau_{\text{gear}} - \alpha\omega, \tag{21}$$

with

$$\tau_{\text{gear}} = \frac{1}{\beta}\mathcal{H}\left(|\dot{\theta}|-\omega\right)\left(|\dot{\theta}|-\omega\right), \tag{22}$$

$$B = \min\left(\max\left(\frac{1}{2}+\gamma-\frac{1}{\epsilon}\sin\theta+\eta\sin(\Omega_w t)\,,\,0\right),\,1\right), \tag{23}$$

where, as in (6), $\mathcal{H}$ is the Heaviside function and β is a small positive number. The above equations are then recast as a first order system

$$\dot{\theta} = \phi, \tag{24a}$$

$$(1+\delta)\dot{\phi} = \epsilon(B-r)\cos\theta - \text{sign}(\phi)\,\tau_{\text{gear}}, \tag{24b}$$

$$\dot{\omega} = \tau_{\text{gear}} - \alpha\omega, \tag{24c}$$

where again ϕ is the angular velocity of the the float.

Unlike the scheme in Subsection 2.3, this scheme does not require "solver-switching" to take place. Instead, the Heaviside term in (6) determines whether or not the gears are engaged. In effect, by checking the sign of $\omega - |\dot{\theta}|$, the Heaviside function outputs zero for the uncoupled case (19); otherwise it gives the coupled equations (18).

The system of equations (24a)-(24c) is an ode system in (θ, ϕ, ω) which is integrated using MATLAB's integrated ode solver[3] and, since MATLAB includes a built-in Heaviside function, this scheme is implemented very easily.

[3]Due to the small values of β, the equations are stiff and MATLAB's ODE solver ode15s is used to integrate in time.

3 Numerical results

In this section, numerical results are presented based on the model of Section 2.3. The first set of results (shown in Figure 5), illustrates a typical example model case with $\delta = 0.0427$, $\epsilon = 0.04$, $\gamma = 0$, $\eta = 1.25$, $r = 0.1$, $\alpha = 0.00066$, and $\Omega_w = 0.0062$. This case shows the motion of the float and flywheel when released from rest with $\omega(0) = 0$, $\theta(0) = 0$, and $\phi(0) = 0$. Evidently, the angular velocity of the flywheel (shown on the top left subfigure), initially includes rapid transient behaviour. However, after roughly one wave period (shown on the bottom right figure), these initial transients have decayed and the angular velocity of the flywheel becomes periodic.

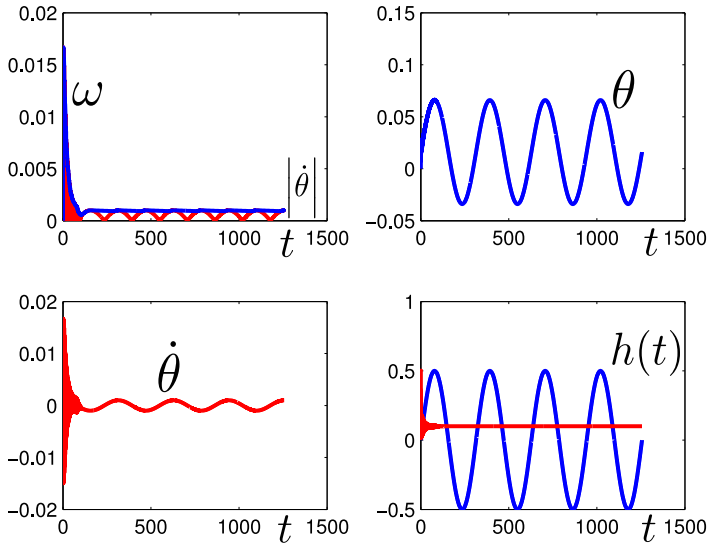

Figure 5: Initial transients as the angular velocity of the flywheel (top left) and angle of the float (top right) are released from rest.

The behaviour in this initial transient regime is dependent of the choice of initial conditions. However, regardless of the choice of initial conditions, the float and flywheel start to demonstrate periodic behaviour after little more than one wave period. The fact that (as in this case), the motion of the float and flywheel become periodic after the float is released from rest with a stationary flywheel is also encouraging: this implies the device is self starting and given the onset of an incoming wave train, the float will start to move, and the flywheel will start to spin regardless of their initial configuration.

3.1 Flywheel evolution and PTO

The evolution of the float and the flywheel are now examined in the periodic regime for a range of different PTO coefficients, α. A case with $\alpha = 0.00066$ is shown in Figure (6). The top left subfigure shows both the angular velocity of the flywheel, ω, and the rectified angular velocity of the float, $|\dot{\theta}|$. When these two quantities are equal, the gearing system is engaged and the wave motion is transferring energy to the flywheel. The parts of the cycle for which $|\dot{\theta}| < \omega$ are also shown. For these times the gears are disengaged, so energy is not transferred to the flywheel. When the gears disengage, the angular velocity of the flywheel decays exponentially, as determined by the $\dot{\omega}$ equation in (19).

The value of the PTO coefficient has a significant effect upon the rate of the decay of the angular velocity of the flywheel. Figure 7 shows the same periodic behaviour for the float and flywheel evolution for $\alpha = 0.0066$ (left) and $\alpha = 0.066$ (right). When compared to Figure 6 (which has $\alpha = 0.00066$), we note that increasing the PTO coefficient, α, hastens the decay in the angular velocity of the flywheel.

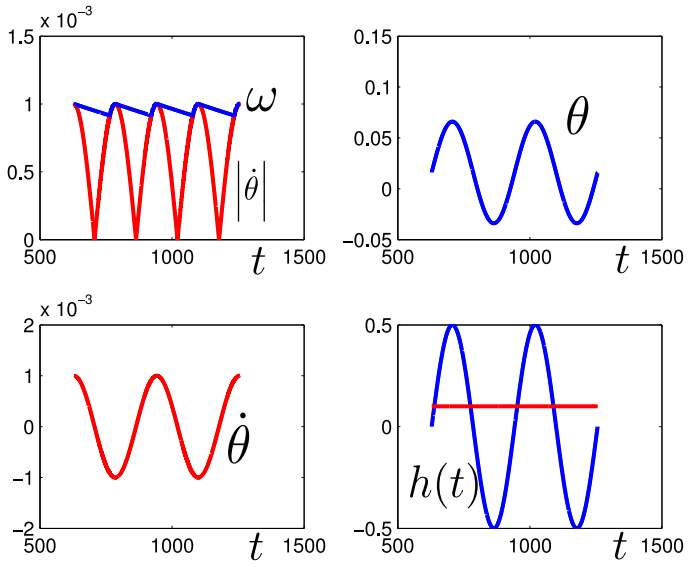

Figure 6: Float and flywheel angular motion for $\alpha = 0.00066$. Showing the angular velocity of the flywheel and the rectified angular velocity of the float (top left), the angle of the float (top right), the angular velocity of the float (bottom left), and the wave height (bottom right).

For the low values of α, shown in Figure 6, the angular velocity of the flywheel retains roughly a constant value of 1×10^{-3} throughout the motion, with only small increases in the angular velocity when the gearing is engaged, and little decay in angular velocity upon disengagement. However, as the PTO coefficient, α, is increased, the rate of decay of the angular velocity of the flywheel increases resulting in a more stop-start angular velocity profile. For the largest value of $\alpha = 0.066$, the flywheel angular velocity decays so rapidly that it follows the rectified angular velocity of the float to such an extent that it is nearly brought to rest at the end of every half wave period, when the vertical motion of the wave changes direction.

The PTO coefficient, α, also has a significant effect on the actual power the device is able to generate. The power P is related to the angular velocity of the flywheel and the PTO coefficient through

$$\dot{P} = \alpha\omega^2. \tag{25}$$

Thus having determined ω, this expression can be integrated to determine the power output. For the three cases presented the power output equals 3.2×10^{-6} when $\alpha = 0.00066$, 2.7×10^{-5} when $\alpha = 0.0066$, and 1.3×10^{-4} when $\alpha = 0.066$. More generally the power output from the device increases with α, which indicates the power generation is greatest when the flywheel is subject to rapid angular accelerations and decelerations rather than roughly constant angular velocity.

3.2 Numerical validation

In Subsection 2.4, an alternative formulation of the problem was outlined. This allows us to compare two different numerical schemes; the results from the original formulation and the alternative formulation are shown in Figure 8. Such good agreement serves as validation of the numerical methods.

4 Ocean-wave power

It is essential to be able to obtain a quantification of the maximum power that can be extracted from the generator for a given wave. The generator is versatile with regards to the varying wave types that it may experience. However, due to certain practicalities and planning restrictions, the analysis presented here is

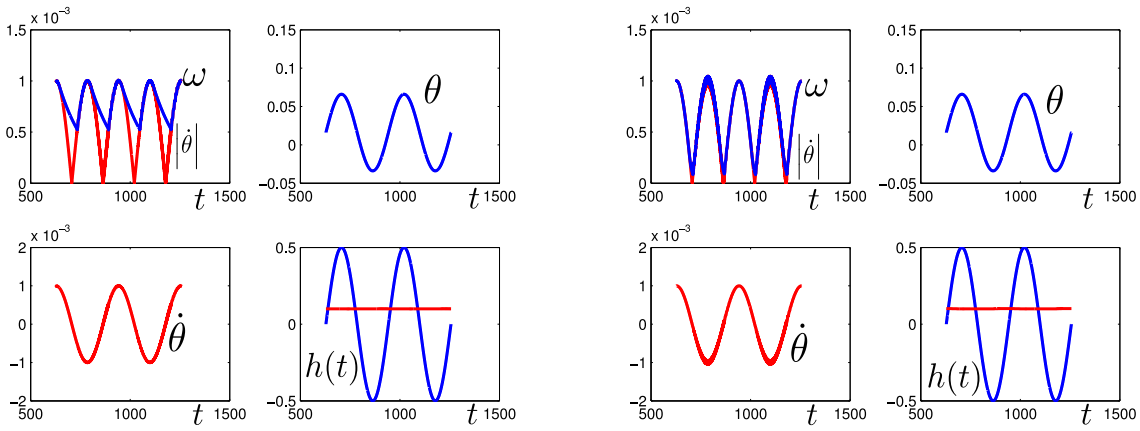

Figure 7: As Figure 6, but showing float and flywheel motion for $\alpha = 0.0066$ (left) and $\alpha = 0.066$ (right).

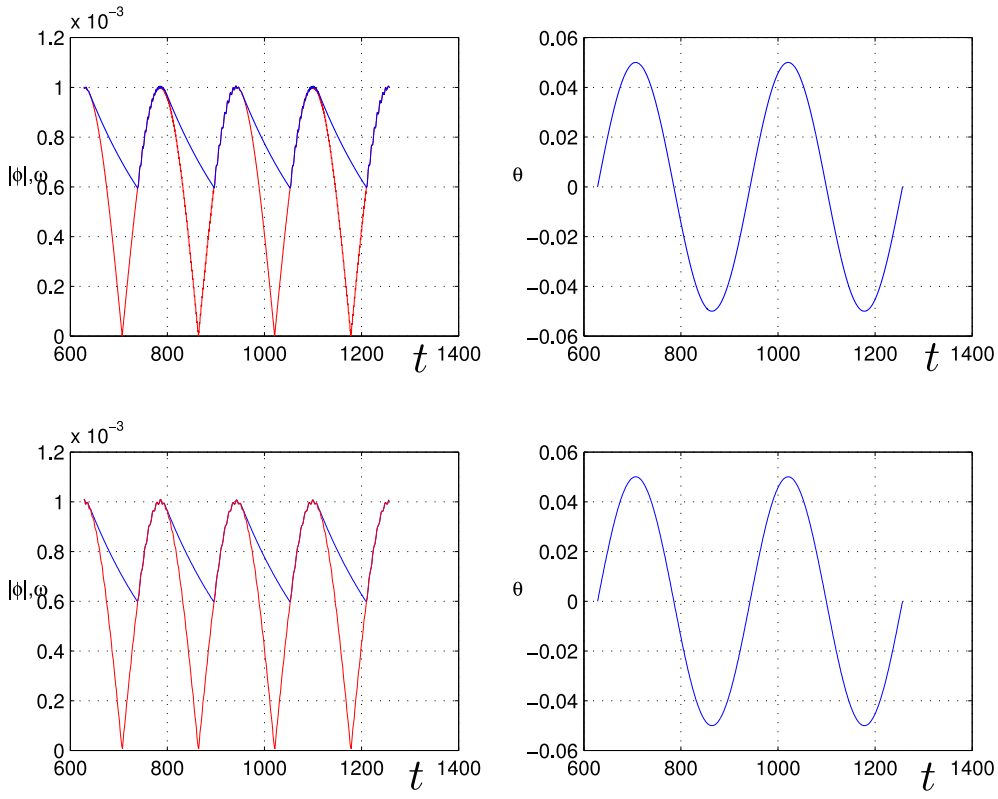

Figure 8: A comparison of the results generated by the numerical method described in Section 2.3 (top), and the alternative numerical scheme described in Section 2.4 (bottom).

based on the generator situated 150 - 200 metres off Galway Bay with a seabed depth of 20 metres. In addition, the wavelength and amplitude of the waves in the sea varies significantly across the seasons. It is therefore necessary to have a generator design that is optimal for all four seasons.

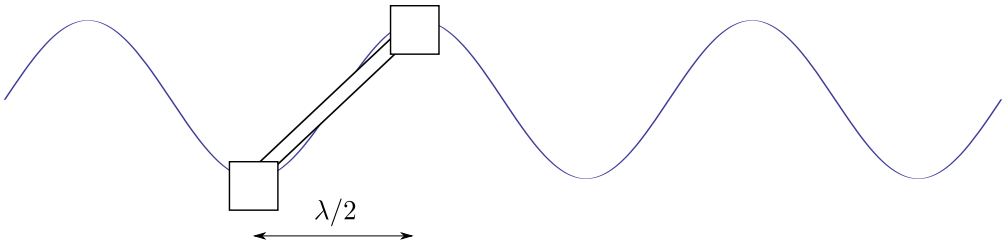

Figure 9: Optimisation of the arm length according to ocean wave data. Placing two points on the sea surface half a wavelength apart will maximise the relative motion.

4.1 Shallow-water model

To carry out the optimisation, we must compute the power delivered by the ocean waves using real wave data. We therefore require an appropriate wave model from which we may compute the corresponding wave power; one such model is the shallow-water equations. These equations rely on the Boussinesq approximation, which, in turn, is valid for the wave data used in this report.

In the shallow-water model, the frequency Ω of a water wave is given by the dispersion relation

$$\Omega^2 = gk \tanh(kh_0), \tag{26}$$

where $k = 2\pi/\lambda$ is the wave number, h_0 is the mean depth of the sea, and g is the gravity constant. It can be shown that the power P delivered to the arm from the wave profile is given by

$$P \propto \ell^2 \Omega^2 \sin^2\left(\frac{\pi L}{\lambda}\right), \tag{27}$$

where ℓ is the amplitude of the wave, λ is its wavelength, and L is the arm length of the device.

4.2 Galway Bay data

To perform the optimisation actual site data was used. The observation buoy at the Galway Bay test site [1] supplies data for the wave height and period, from which one can easily obtain Ω and ℓ (see Figure 10). Data sets for each season were used in the analysis in order to examine both the variation in the different components and to find an arm size optimal for each season. To obtain values for wavelengths λ, MATLAB was used to solve (26) numerically for λ (with depth $h_0 = 20$ m), which was then used in (27) to solve for the relationship between the Power P and the arm length L. This approach allowed for the optimal L to be found. The outcome of the analysis is presented for the wave height, frequency, and length in Figure 11.

From Figure 11, one can see that the wave properties, and therefore the generated power, vary significantly over a year. This needs to be taken into consideration when designing the device shape and scale. The device is more likely to generate maximal output in the winter due to the greater wave amplitude. However, the arm length that is optimal for the maximum energy generation in the winter is not entirely optimal for the other seasons. One solution would be to have an arm length which could be varied throughout the year. However, this may not be practical from a financial viewpoint. The most feasible alternative is to choose an arm length which is a "best-fit" for all four seasons. From Figure 12, we conclude that at a length $L \approx 14$ m maximum power will be extracted for the given season. This length is also very reasonable from a structural viewpoint.

5 Conclusions

In this report we have presented a simple mathematical model for Limerick Wave's WEC device. At present, Limerick Wave has a working, 1:20 scaled device; testing larger rigs is costly so this model will play a crucial role in the design of the scaled-up version. In particular, the model enables tuning of the device

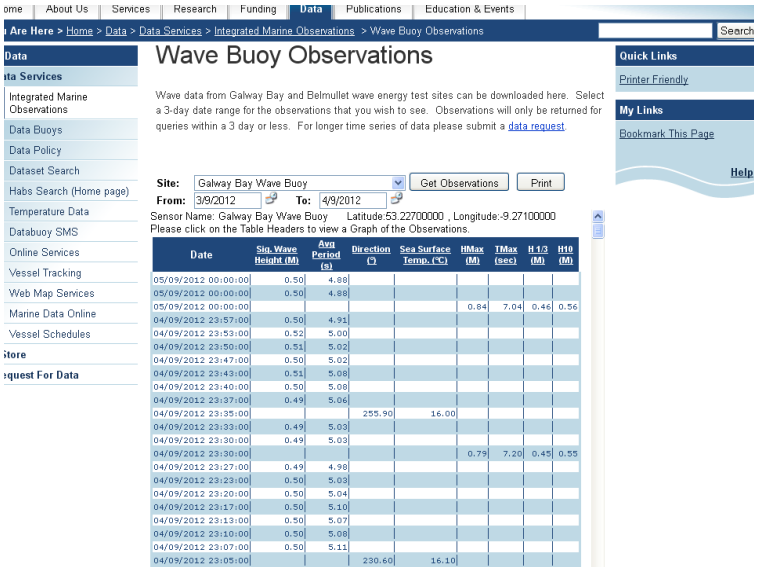

Figure 10: Sample data lookup at [1].

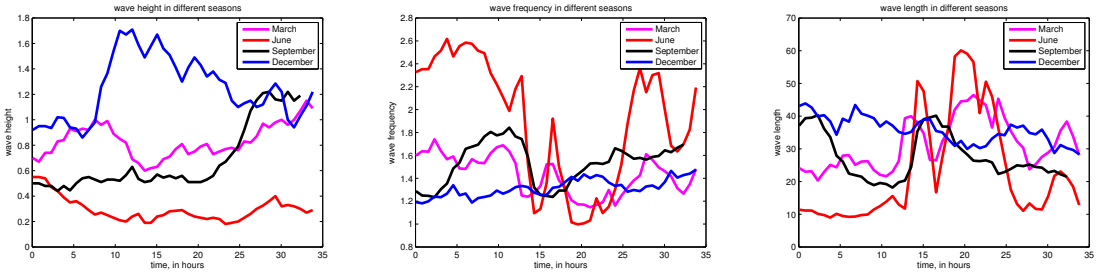

Figure 11: Sample wave height, frequency, and length for the different seasons. Data for the dates: 3-4/03/2012, 3-4/06/2012, 3-4/09/2012, 3-4/12/2012.

to optimise the energy extracted from waves of different frequencies and amplitudes. For further work we suggest studying the real data in greater detail since it is crucial for the efficiency of the device.

The model comprises two coupled ordinary differential equations which, in turn, represent conservation of angular momentum during the operation of the device. The model also incorporates the interaction (buoyancy, weight, and inertia) between the floatation device and the incoming water waves.

We investigated, in detail, two operating states: when a large proportion of the energy is extracted per cycle (large PTO) and when a small portion of the energy is extracted (small PTO). In the latter case, the flywheel could be kept spinning at an almost constant angular velocity and hence an almost constant current can be extracted. In the former case, the flywheel follows the arm's (and hence the original wave's) movement. The trade-off to requiring a large PTO is the high variability of the output current.

A separate analysis was carried out for the optimisation of the device's arm length. We considered wave data from Galway Bay and used the shallow-water dispersion relation to approximate the wave frequency which in turn determines the power delivered to the device. For the sake of simplicity, in this part of the analysis we assumed that the device is untethered. We find that the maximum amount of power is extracted when the device's arm is one half the wavelength of the incoming waves. The wave data has a strong seasonal variation so a best-fit of the four seasons is computed giving an optimal arm length of 14 metres across the seasons.

The mathematical model contains a number of dimensionless parameters; some of these were small or are operational parameters which should be tweaked. Although it was not carried out here, some of these

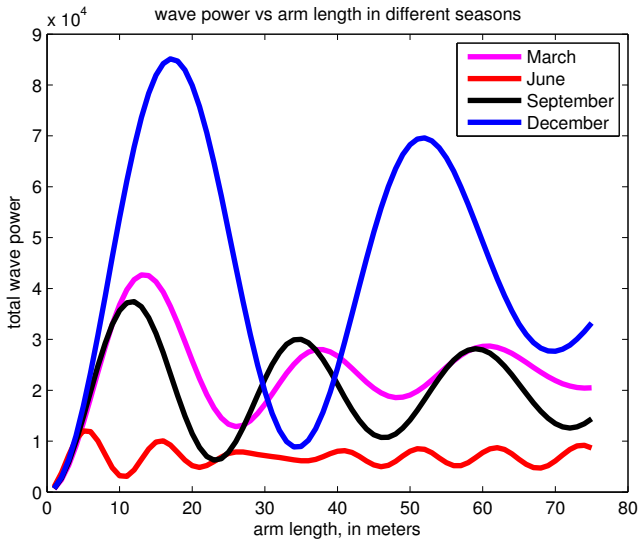

Figure 12: Maximum power generated by waves for the different seasons. Data for the dates: 3-4/03/2012, 3-4/06/2012, 3-4/09/2012, 3-4/12/2012.

parameters may be determined through the Galway Bay power-optimisation analysis. Other future work should include an analysis of the full hydrodynamic model and a tethered power analysis.

Acknowledgements

The authors acknowledge support of the Mathematics Applications Consortium for Science and Industry (www.macsi.ul.ie) funded by the Science Foundation Ireland (SFI) Investigator Award 12/IA/1683, the SFI Conference and Workshop grant 13/CW/12578, and the Enterprise Ireland Innovation Voucher Scheme. We are also grateful to Dr. Paddy Walsh for his help, patience, and direction during the week.

References

[1] http://www.marine.ie/home/publicationsdata/data/IMOS/WaveBuoyObservations.htm.

[2] Alain Clément, Pat McCullen, António Falcão, Antonio Fiorentino, Fred Gardner, Karin Hammarlund, George Lemonis, Tony Lewis, Kim Nielsen, Simona Petroncini, M.-Teresa Pontes, Phillippe Schild, Bengt-Olov Sjöström, Hans Christian Sørensen, and Tom Thorpe. Wave energy in Europe: current status and perspectives. *Renewable and Sustainable Energy Reviews*, 6(5):405–431, 2002.

[3] António F. de O. Falcão. Wave energy utilization: A review of the technologies. *Renewable and Sustainable Energy Reviews*, 14(3):899–918, 2010.

[4] Johannes Falnes. A review of wave-energy extraction. *Marine Structures*, 20(4):185–201, 2007.

[5] John B. Herbich. *Handbook of Coastal and Ocean Engineering, Vol. 1: Wave Phenomena and Costal Structures*. Gulf Pub. Co, 1991.

[6] S. K. Wilson. A mathematical model for the initial stages of fluid impact in the presence of a cushioning fluid layer. *J. Eng. Math.*, 25(3):265–285, 1991.